NOAA Technical Memorandum ERL WPL-186

DUAL-FREQUENCY RADAR: BASIC THEORY AND SURFACE CURRENT MAPPING PERFORMANCE FOR LAND-BASED SYSTEMS

A. Jay Palmer

Wave Propagation Laboratory
Boulder, Colorado
October 1990

noaa NATIONAL OCEANIC AND ATMOSPHERIC ADMINISTRATION / Environmental Research Laboratories

NOAA Technical Memorandum ERL WPL-186

DUAL-FREQUENCY RADAR: BASIC THEORY AND SURFACE CURRENT MAPPING PERFORMANCE FOR LAND-BASED SYSTEMS

A. Jay Palmer

Cooperative Institute for Research in Environmental Sciences
University of Colorado
Boulder, Colorado

Wave Propagation Laboratory
Boulder, Colorado
October 1990

UNITED STATES
DEPARTMENT OF COMMERCE

Robert A. Mosbacher
Secretary

NATIONAL OCEANIC AND
ATMOSPHERIC ADMINISTRATION

John A. Knauss
Under Secretary for Oceans
and Atmosphere/Administrator

Environmental Research
Laboratories

Joseph O. Fletcher
Director

NOTICE

Mention of a commercial company or product does not constitute an endorsement by NOAA/ERL. Use of information from this publication concerning proprietary products or the tests of such products for publicity or advertising purposes is not authorized.

For sale by the National Technical Information Service, 5285 Port Royal Road
Springfield, VA 22161

CONTENTS

DUAL-FREQUENCY RADAR: BASIC THEORY AND SURFACE CURRENT MAPPING PERFORMANCE FOR LAND-BASED SYSTEMS

A. Jay Palmer

ABSTRACT--I review the essential theoretical aspects of dual-frequency radar sensing of ocean surface currents. The review includes the basic single carrier frequency technique as well as the multiple carrier frequency technique used to improve the signal-to-noise ratio. I add to this review my calculation of the dependence of the signal-to-noise ratio on a finite time separation between the transmitted radar signals, and my calculations of the achievable surface-current resolution for land-based systems. Scaling relationships and resolution contours are plotted, which will help in the design of an optimal current mapping system. I conclude with a brief discussion of two new dual-frequency radar concepts: bistatic dual-frequency radar and dual-frequency sodar.

1. INTRODUCTION

1.1 Objectives

The objectives of this technical memorandum are to present a consolidated theoretical description of the dual-frequency radar concept (also referred to as Δk radar) and to use this description to predict the measurement resolution of ocean surface current using a land-based Δk radar. These objective are addressed in Sections 2 and 3, below. The material in Sections 2.1 and 2.2 is a review of already published theory. To my knowledge, the material in Sections 2.3, 3, and 4 is original. In particular, the scaling relationships appropriate to the finite-footprint broadening of the Δk line are new, and have, together with the analysis of the bistatic Δk-radar concept, been submitted for journal publication.

1.2 History

The Δk radar technique was developed as a compact remote sensing technique for measuring ocean currents and surface wave spectra. Most of the pioneering work on this concept has been reported out of the Naval Research Laboratories, the principal workers being W. Plant and D. Schuler. The first comprehensive study of this technique, both experiment and theory, was published by Plant in 1976[1]. Several papers by Plant, Schuler, and others followed[2,3,4]. This series of works culminated with a paper in 1985 by R. McIntosh and coworkers[4] which presented a broad systems analysis and optimization study for applying the technique to the measurement of ocean currents from satellites.

Since then, the only significant conceptual advance for the technique came in 1985 when Schuler, Plant, and coworkers[5] published a paper demonstrating theoretically and experimentally the ability of frequency agility to improve the signal-to-noise ratio.

1.3 Heuristic Description

The basic procedure behind Δk radar is to scatter from the ocean surface two microwave beams that are at two different frequencies. By detecting the low-frequency component of the product of the two scattered fields, one is able to determine the frequency and wavenumber of an ocean swell. The measured departure of the dependence of frequency on wavenumber from the known dispersion law for ocean swells gives a measure of the current component along the radar look direction.

In this technique, the microwave fields are backscattered dominantly by capillary waves whose wavevectors satisfy the Bragg condition, in which the wavenumber of the capillary wave is equal to twice the magnitude of the surface-projected wavevector of the microwave radiation. The presence of an ocean swell modulates (temporally and spatially) the amplitude, slope, and wavenumber of the capillary waves. (The microwave path length is also modulated by the swell, but this can usually be neglected.) These modulations cause a corresponding modulation of the scattered microwave fields.

Clearly, the temporal modulation of a swell could be detected on just a single scattered microwave field by a radar having a range resolution much finer than the swell wavelength. This is done in the so-called two-scale wave probe[2]. The advantage of detecting the product of two frequency separated, scattered microwave fields to determine the parameters of the swell is that there is a spatial coherence factor in the expression for the scattered product field that singles out a particular ocean swell wavevector. Physically, this coherence factor comes about because of the same type of phase coherence that dictates the Bragg condition for coherent scattering of the individual microwave fields. However, it is important to recognize that Δk radar is not equivalent to single-frequency Bragg scattering off an ocean swell by a radio frequency (RF) field. In the absence of a swell, a scattered microwave product-field will still exist, whereas a Bragg-scattered RF field will vanish.

Now let us consider the temporal behavior of the received product field. First consider the case of a continuous wave (CW) transmitted beams. What do we expect the temporal spectrum to look like for frequencies much lower than the product-field fundamental frequency? (The fundamental is the frequency difference of the two microwave fields.) In the absence of ocean

swells, we expect to see simply a broad spectrum of noise as the Bragg-resonant capillary waves oscillate and decay over an essentially unconstrained, wide range of characteristic time scales. Now, consider that there is an ocean swell present which happens to satisfy the above Bragg condition for the transmitted product-field wavevector. Then we expect the phase coherence between the product field and the swell-induced modulation factor to maximize at a position in the temporal spectrum of the received product field that corresponds to a traveling wave component in the product field moving synchronously with the swell. Since the Bragg-resonant ocean swell has a unique frequency, unlike the capillary waves, this phase coherence maximum will be manifested as a single resonance line in the temporal Fourier spectrum of the autocovariance of the received product field. Since a pulse train can also be decomposed into traveling-wave components, the autocovariance of a received product-field pulse train will also reveal the same phase-coherence resonance line in its temporal Fourier spectrum. Because the ocean current adds to the phase velocity of the swell, a measurement of the frequency of this line gives a measure of the current.

2. THEORY OF OPERATION: SIGNAL-TO-NOISE RATIOS

2.1 Basic Dual-Frequency Theory

Consider two microwave beams with wavevectors $\mathbf{k}_1$ and $\mathbf{k}_2$ scattered simultaneously from a patch of ocean surface defined by an antenna footprint $f(\mathbf{r})$, as depicted in Fig. 1. The magnitude of the individual scattered fields is given by

$$E_i = C_1 \exp(2i\mathbf{k}_i \cdot \mathbf{r}_o) \int f(\mathbf{r})\ h(\mathbf{r},t)\ \gamma(\mathbf{r},t)\ \exp(i2\mathbf{k}_i \cdot \mathbf{r})\ d\mathbf{r} \tag{1}$$

where C is proportional to the backscatter cross section per unit area for microwave scattering by capillary waves of unit amplitude, γ is the amplitude of the capillary waves undisturbed by swells, h is a multiplier of this amplitude assumed to account for the effects of the swells, and the exponents contain the relevant phase factors for the scattering.

Now consider sensing the product of the two scattered fields using an analogue or digital mixer. The low-frequency part of this product signal, which can be separated with a low-pass filter, is given by $(E_1\ E_2^*)$, where $E_{1,2}$ are given by Eq. (1). Finally, consider processing this signal further by forming its power spectrum given by

$$P(\omega) = \int \overline{E_1(t)\ E_2^*(t)\ E_1(t+\tau)\ E_2^*(t+\tau)}\ \exp(i\omega\tau)\ d\tau \tag{2}$$

where the bar indicates time average.

If one makes use of the fact that $\gamma(\mathbf{r},t)$ has zero mean and zero cross correlation for large spatial separations, then the integrations in Eqs. (1) and (2) are straightforward and yield[1]

$$\begin{aligned} P(\omega) = |C_1 C_2|^2 \Big\{ & B \int \psi(2k_1, \omega')\ \psi(2k_2, \omega - \omega')\ d\omega' \\ & + \psi(2k_2)^2 \int |f(\mathbf{r})|^2\ |f(\mathbf{r}+\mathbf{q})|^2 \\ & \times |h(\mathbf{r},t)|^2\ |h(\mathbf{r}+\mathbf{q}, t+\tau)|^2 \\ & \times \exp[-i(2\Delta\mathbf{k} \cdot \mathbf{q} + \omega\tau)]\ d\mathbf{q}\, d\mathbf{r}\, d\tau \Big\} \end{aligned} \tag{3}$$

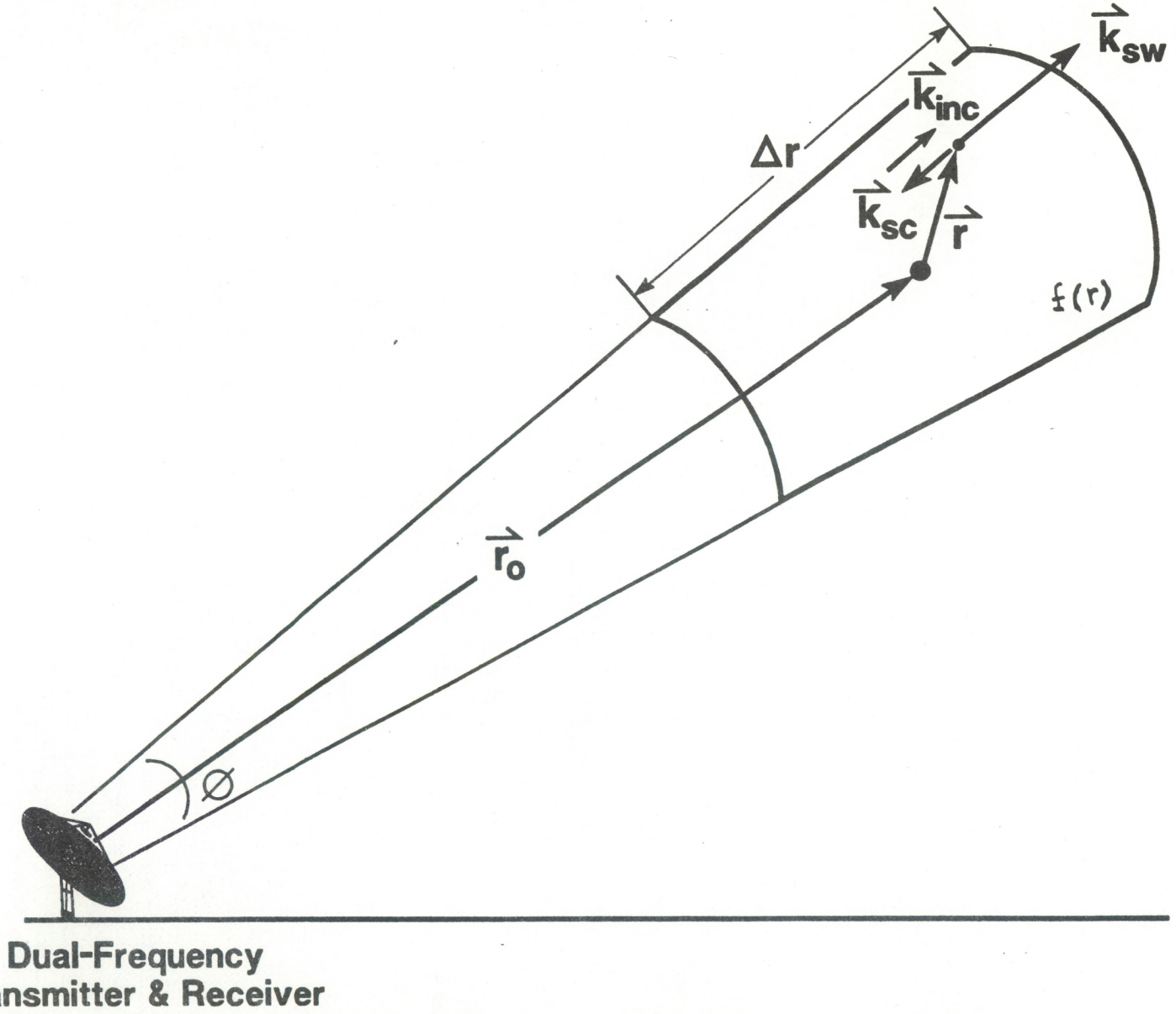

Figure 1. Dual-frequency radar sensing of the ocean surface.

where ψ is the power spectrum of γ, and

$$B = \int |f(\boldsymbol{r})|^2 \; |f(\boldsymbol{r}')|^2 \; |h(\boldsymbol{r}, t)|^2 \; |h(\boldsymbol{r}', t)|^2 \; d\boldsymbol{r}\, d\boldsymbol{r}' \tag{4}$$

The first term in Eq. (3) represents a broad background spectrum, whereas the second, if a dispersion relation exists for $h(\mathbf{k},\omega)$, represents a sharp line at a frequency corresponding to

$$\omega = \omega(2\Delta k) \; . \tag{5}$$

If we now integrate Eq. (3) over ω, and divide the second term by the first, we obtain a signal-to-noise ratio defined as the energy in the scattered Δk resonance line divided by the energy in the scattered background radiation:

$$\chi = \frac{\int f(2\Delta\boldsymbol{k} - \boldsymbol{k})\; H(\boldsymbol{k})\; d\boldsymbol{k}}{\int f(-\boldsymbol{k})\; H(\boldsymbol{k})\; d\boldsymbol{k}} \tag{6}$$

where

$$H(\boldsymbol{k}) = \int H(\boldsymbol{r}, t)\; H^*(\boldsymbol{r} + \boldsymbol{q})\; \exp(-i\,\boldsymbol{k}\cdot\boldsymbol{q})\; d\boldsymbol{q} \; . \tag{7}$$

The function $H(\mathbf{k})$ accounts for the modulating effect of the swells on the microwave scattering from the capillary waves. A similar function called the modulation transfer function, m, enters the expression that relates the individual microwave backscattered power from the capillary waves to the orbital motion of the swells. Since this modulation transfer function is a more commonly measured quantity for the ocean surface than H, it is useful to express H in terms of m. This is done in Ref. (2). If this substitution is made together with the assumption that the antenna pattern, $f(\boldsymbol{r})$, is large compared to the swell wavelength, then Eq. (6) is shown in Ref. (2) to reduce to

$$\chi = \frac{2\pi^2 \; |m(ksw)|^2 \; k_{sw}^2 \; F(k_{sw}) \; \coth(k_{sw}d)}{A} \; . \tag{8}$$

where k_{sw} is the Bragg-resonant swell wavenumber which, for backscattering, satisfies

$$k_{sw} = 2\Delta k \ . \tag{9}$$

$F(k_{sw})$ is the power spectrum of the swells in units of length to the fourth power, and A is the area of the illumination pattern.

2.2 Multiple Frequency Generalization

In the above review, the analyzed output signal was the power spectrum of the autocovariance (auto-spectrum) of the low frequency product of two frequency-separated microwave fields scattered from the ocean surface. We now consider the power spectrum of the cross covariance (cross-spectrum) of the low-frequency product of two frequency-separated microwave fields between pairs with different carrier frequencies. It can easily be shown[5] that this cross-spectrum is identical to the auto-spectrum given by Eq. (3) except that the integrand for the factor B in Eq. (4) obtains an added phase factor

$$\exp(i2\,\boldsymbol{\delta k}\cdot\boldsymbol{\rho}) \tag{10}$$

where $\boldsymbol{\delta k}$ is the carrier wavevector difference between the two pairs of scattered fields. The appearance of this phase factor causes the signal-to-noise ratio given by Eq. (6) to change to

$$\chi(\boldsymbol{\delta k}) = \frac{\int f(2\Delta k - k)\ H(k)\ dk}{\int f(\boldsymbol{\delta} k - k)\ H(k)\ dk} \tag{11}$$

After the substitutions for H(k) in terms of the modulation transfer function as before, the signal-to-noise ratio becomes:

$$\chi(\boldsymbol{\delta} k) = \frac{|m(k_{sw})|^2\ k_{sw}^2\ F(k_{sw})\ \coth(k_{sw}d)}{|m(\boldsymbol{\delta} k)|^2\ (\boldsymbol{\delta} k)^2\ F(\boldsymbol{\delta} k)\ \coth(\boldsymbol{\delta} kd)} \tag{12}$$

Comparing Eq. (12) with Eq. (8), it is seen that an increase in the signal-to-noise ratio is achieved over the signal carrier frequency result for

$$A > 2\pi^2 \, |m(\delta k)|^2 \, (\delta k)^2 \, F(\delta k) \coth(\delta k d) \; . \tag{13}$$

It is important to recognize that the signal-to-noise ratios given by Eqs. (8) and (12) are defined in terms of time averages of random data records. In particular, the cross-spectrum background signal, proportional to the denominator of Eq. (12), can never have a statistically significant smaller value than its variance. But the variance, σ, of a cross-spectrum of a signal obeys the general relationship

$$\sigma \sim \frac{2\pi G(\omega)}{\sqrt{n}} \tag{14}$$

where $G(\omega)$ is the autospectrum and n is the number of independent records. Thus,

$$\chi(\delta k) < \frac{\sqrt{n}\,\chi(0)}{(2\pi)} \tag{15}$$

Larger δk values tend to increase χ given by Eq. (12), but in practice, they decrease n and thereby decrease the upper limit to χ given by Eq. (15).

2.3 Sequential Frequency Generalization

Throughout the above analysis, it was assumed that the two members of the dual-frequency pairs of microwave signals were transmitted simultaneously. We now generalize the analysis to the case of transmitting the dual-frequency signals with a time separation, T.

T makes its appearance in carrying out the time averages in Eq. (2). It does not appear in the temporal integration of the background term because there it just adds to the integration variable, τ. The only place that T appears after carrying through the time averages is in the second term of Eq. (3), which is the Δk resonance line term. Here the only change is that the capillary wave auto-spectrum becomes a cross-spectrum:

$$\Psi(2k_2) \rightarrow \Psi(2k_2, T) \; . \tag{16}$$

After the frequency integration is performed to obtain the spectrally integrated signal-to-noise ratio, the capillary wave

power spectrum will not cancel out as before, and one is left with

$$\chi(T) = \chi(T=0) \frac{[\Psi(2k_2, T)]}{[\Psi(2k_2, 0)]} . \qquad (17)$$

This can be written in terms of the capillary wave decorrelation rate of the Bragg resonant capillary waves, $\Gamma(2k_2)$:

$$\chi(T) = \chi(T=0) \exp[-\Gamma(2k_2) T] . \qquad (18)$$

Thus, as long as the two dual-frequency signals are transmitted within a time separation that is small compared to the decorrelation time, the signal-to-noise ratio will remain unchanged from that for the case of simultaneous transmission. It will fall exponentially as the time separation exceeds the decorrelation time.

3. THEORY OF OPERATION: SURFACE CURRENT RESOLUTION

3.1 Single-Station Resolution

As reviewed above, since an ocean swell has a unique dispersion relationship, the power spectrum of the scattered product-field for two dual-frequency microwave beams will contain a resonant peak at a frequency equal to the Doppler-shifted frequency of the swell whose wavevector satisfies the Bragg condition given by Eq. (9). This frequency is given by

$$\nu = \nu_o + \boldsymbol{k}_{sw} \cdot \boldsymbol{v}/2\pi \tag{19}$$

where $\boldsymbol{v}$ is the local ocean current and ν_0 is the zero current frequency of the swell given by

$$\nu_o = \frac{[g\, k_{sw} \tanh (k_{sw} d)]^{12}}{(2\pi)} \quad . \tag{20}$$

Here g is the acceleration of gravity and d is the water depth. Thus, a measure of the frequency of the Δk resonance line gives a measure of the current component along the Bragg-resonant propagation vector of the swell.

The accuracy with which one can measure the center frequency of the Δk resonance line, and hence the current component, will depend on the signal-to-noise ratio of the line and on the width of the line. If we assume that the line is Gaussian with a 1/e width of $\gamma_{\Delta k}$, then differentiation of this Gaussian with respect to the center frequency reveals that the uncertainty in locating the center frequency of the line due to presence of noise is given by

$$\delta\nu = \frac{\gamma_{\Delta k}}{[2\,(S/N)\,]^{1/2}} \tag{21}$$

where S/N is the ratio of the average amplitude of the line to the root-mean-square amplitude of the noise. Using Eq. (9), this corresponds to an uncertainty of the measured current component along $\boldsymbol{k}_{sw}$ of

$$\delta v = \frac{(\gamma_{\Delta k}/k_{sw})}{[2\,(S/N)\,]^{1/2}} \tag{22}$$

The signal-to-noise ratio that enters Eqs. (21) and (22) is related to the spectrally integrated signal-to-noise ratio, $S/N|_{int}$, derived in the previous sections by

$$S/N = S/N|_{int} \, (\gamma_N/\gamma_{\Delta k}) \tag{23}$$

where γ_N is the spectral width of the noise background.

To complete our calculation of the current resolution, we must determine the frequency width, $\gamma_{\Delta k}$, of the Δk resonance line that enters into Eqs. (22) and (23). For an airborne or space-based dual-frequency radar, the Δk line width is dominated by finite aperture, Doppler broadening[4]. For stationary land-based systems, the line width will usually be controlled by the finite extent of the resolved ocean surface pixel along the propagation direction of the swell. If the surface illumination pattern is assumed to be Gaussian along the swell propagation vector, then the shape of Δk line will also be gaussian. The line width in wavenumber space is then

$$\delta k = \frac{1}{\Delta r} \tag{24}$$

where Δr is the 1/e illumination width along $\mathbf{k}_{sw}$. This line width can be derived from Eq. (3) above or see Eqs. (18) and (19) of Ref. (3). Equation (24) corresponds to a frequency line width for the Δk line of

$$\gamma_{\Delta k} = \frac{[2 \, g \tanh(k_{sw} d) \, / \, \Delta r]^{1/2}}{(2\pi)} \, . \tag{25}$$

Combining Eqs. (22) and (25), the uncertainty in the current component measurement becomes

$$\delta v = 1/k_{sw} \left\{ \frac{g \tanh(k_{sw} d)}{[\Delta r \, (S/N)]} \right\}^{1/2} \tag{26}$$

If we now substitute Eqs. (22), (23) and (25) into Eq. (26), we have, for the achievable current resolution,

$$\delta v = \left\{ \frac{g^{3/2} \tanh^{7/2}(k_{sw} d)\, r\phi}{\left[2^{3/2} \pi^3 k_{sw}^4 \Delta r^{1/2} n^{1/2} |m(k_{sw})|^2 F(k_{sw}) \gamma_N \right]} \right\}^{1/2} \qquad (27)$$

where we have allowed for n averaged, statistically independent spectra and have used for the area of the resolved pixel

$$A = r\phi \Delta r \ . \qquad (28)$$

Equation (27) gives the measurement resolution of the surface current component along the propagation vector of the Bragg-resonant ocean swell, which, for a monostatic Δk radar, is along the radar look direction. Using the nominal set of ocean surface parameters presented in Table 1, a deep water assumption, and an assumed antenna beamwidth of $\phi = 0.8°$, δv is computed from Eq. (27) and is plotted in Fig. 2 as a function of range for selected values of the product of $(n \Delta r)$. The vertical asymptotes simply depict the range beyond which the grazing angle reduces the radar cross section rapidly to zero.

Table 1: Ocean surface parameters used for computation of surface current resolution	
σ	-25 dB
$F(k_{sw})$	$.05\ k_{sw}^{-4}$
$m(k_{sw})$	13
γ_N	100 Hz

For the chosen Phillip's spectrum for $F(k_{sw})$, δv is independent of k_{sw}. The ocean swell wavenumber being observed will, of course, be determined by the chosen frequency difference for the microwave beams through the Bragg condition, Eq. (9). The observed swell wavenumber will, in turn, determine the minimum observation time, T_{obs}, required to achieve a given velocity resolution. This determination is given by the time-frequency uncertainty principle as

$$T_{obs} > \frac{2\pi}{(k_{sw} \delta v)} \ , \qquad (29)$$

and is plotted in Fig. 3.

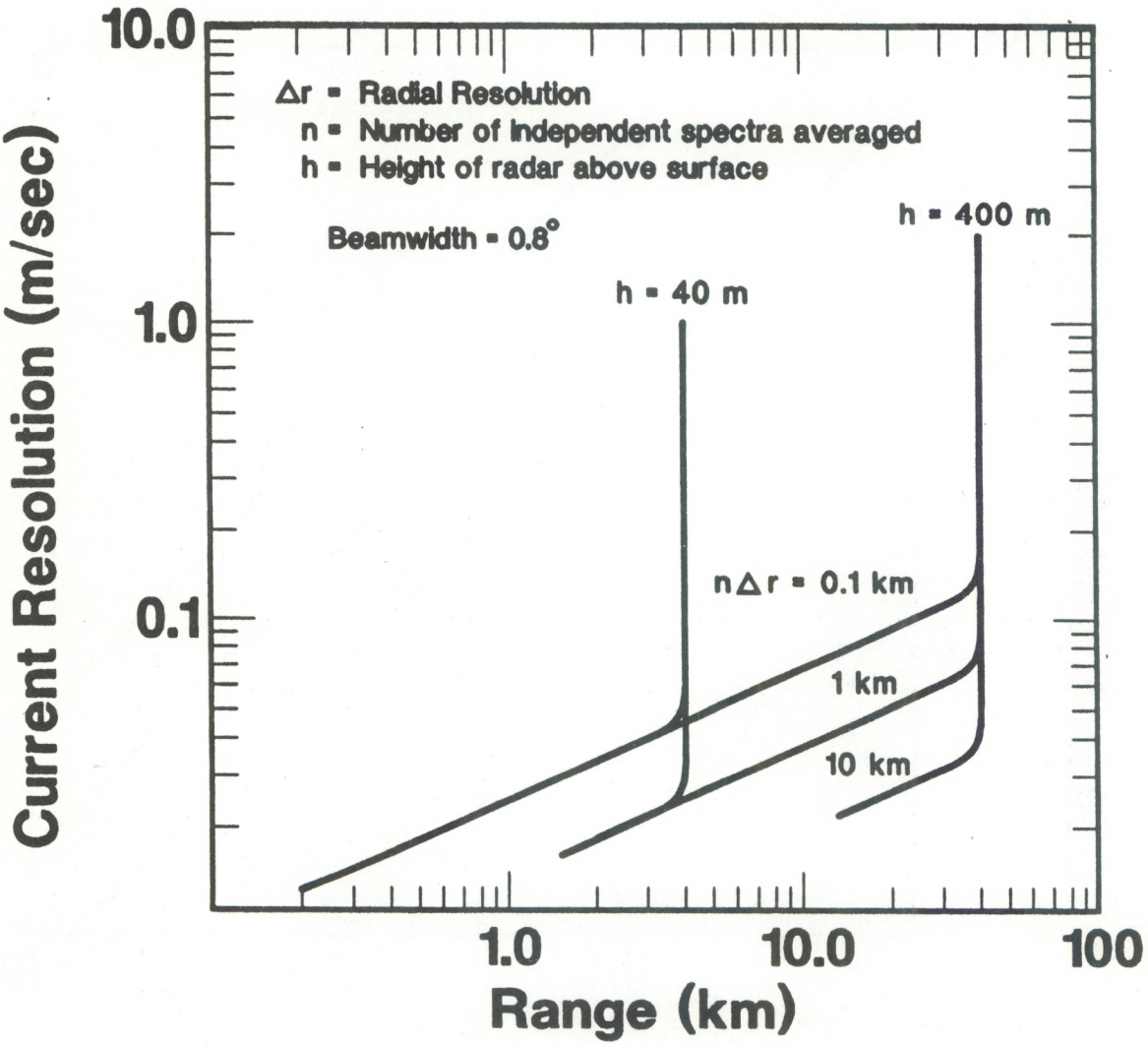

Figure 2. Achievable surface current resolution along radar look direction for surface conditions listed in Table 1.

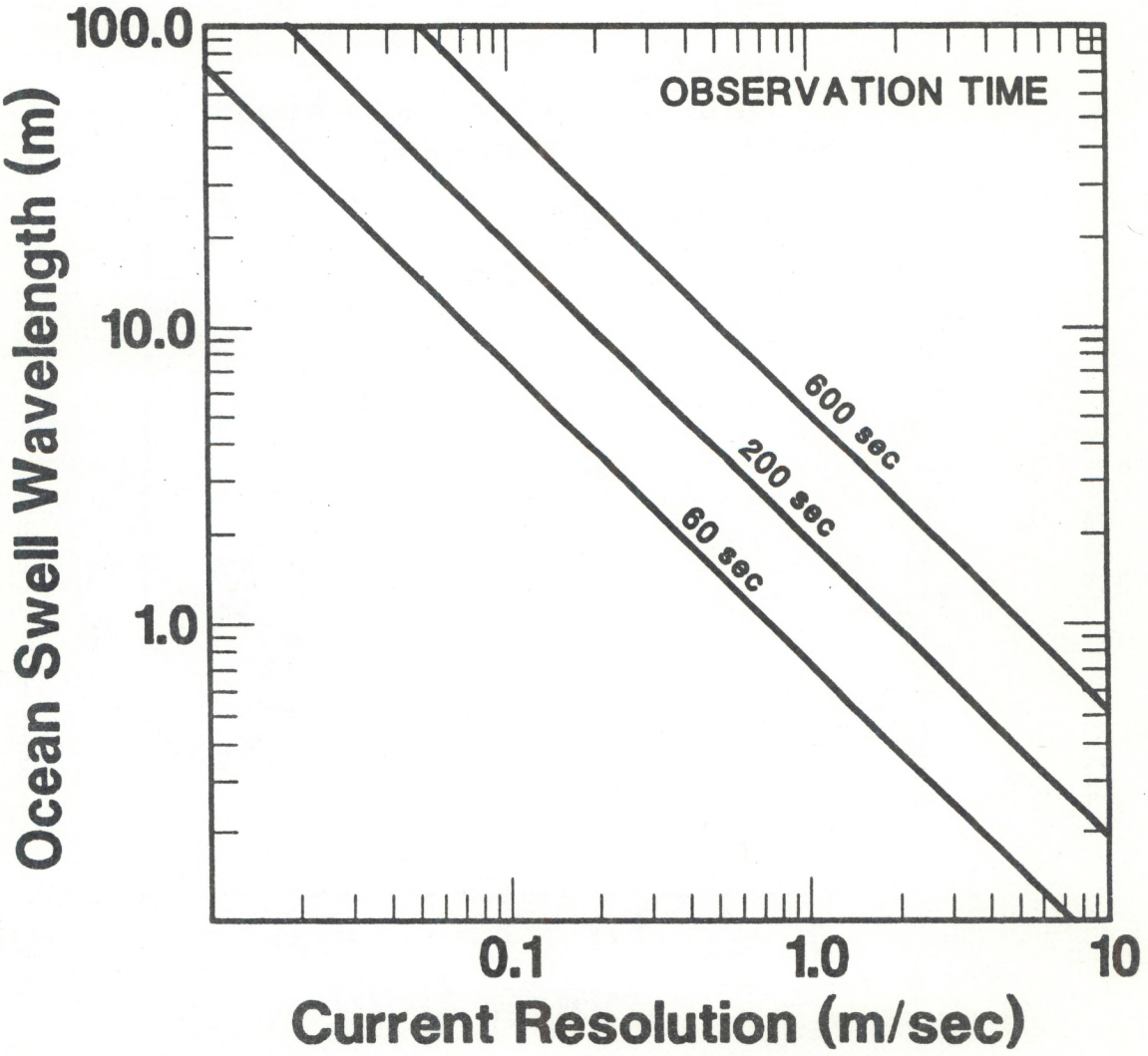

Figure 3. Surface current resolution vs. selected swell wave length for various observation times [from Eq. (29)].

Finally, for whatever measurement parameters selected, one must be assured that the amplitude signal-to-noise ratio itself remains high enough to identify the Δk resonance line within the background noise spectrum. The threshold signal-to-noise ratio required for this will depend on the particular algorithm used in the signal processing. By using Eqs. (21) and (25), the required signal-to-noise ratio can be plotted as a function of Δr with only the observation time as a parameter. This plot is shown in Fig. 4.

3.2 Two-Station Surface Current Resolution

Any Doppler radar system that attempts to measure a velocity field in two dimensions must obtain velocity components in at least two noncollinear directions. The continuity equation can be used to permit a single Doppler radar to obtain a two-dimensional ocean surface current field[6]. However, the use of the continuity equation generally produces a much coarser resolution of the velocity field than does the addition of another radar. In this section we compute the resolution of an ocean surface current vector field made possible with two spatially separated, monostatic, Δk-radar installations. The application of a bistatic Δk-radar configuration to this problem is analyzed in Ref. 7 and discussed briefly in Section 4.1.

Before we can compute the resolution of the measured current field, we must add to the above formulas the vector decomposition relationships for obtaining the current components along two orthogonal axes in terms of the measured current components along the two Bragg-resonant swell propagation directions. For the x and y axis components illustrated in Fig. 5, these relations are

$$v_x = \frac{[v_1 \sin(\theta_2) - v_2 \sin(\theta_1)]}{\sin(\theta_2 - \theta_1)} \tag{30}$$

$$v_y = \frac{[-v_1 \cos(\theta_2) + v_2 \cos(\theta_1)]}{\sin(\theta_2 - \theta_1)} \tag{31}$$

where v_1 and v_2 are the current components measured along $\mathbf{k}_{sw}$ for the two Δk-radar stations. The uncertainty of the current vector along the x and y directions is taken as the root mean square of the uncertainties contributed by v_1 and v_2 measurement uncertainties:

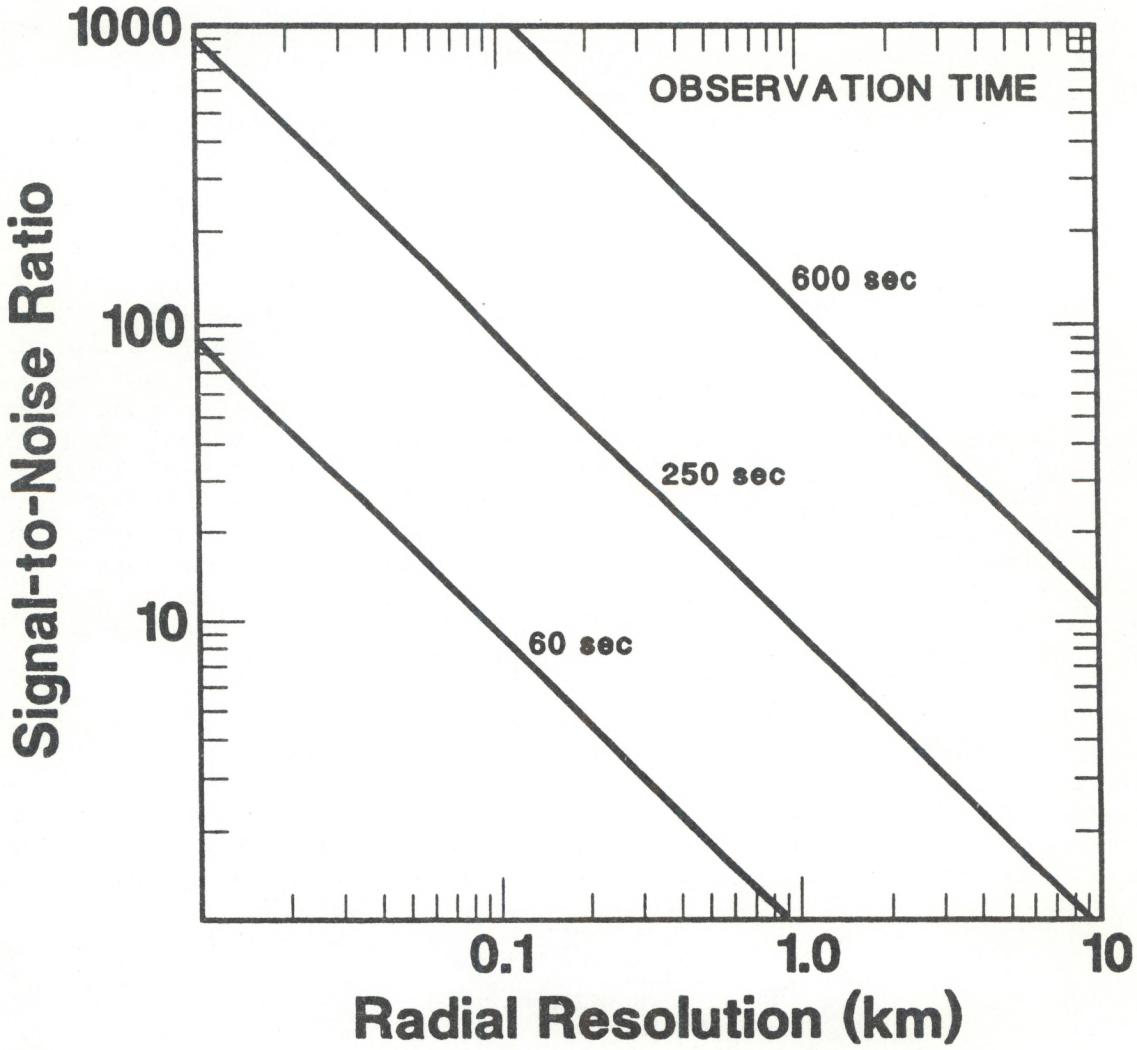

Figure 4. Required amplitude signal-to-noise ratio vs. desired radial resolution for various observation times [from Eqs. (21) and (25)].

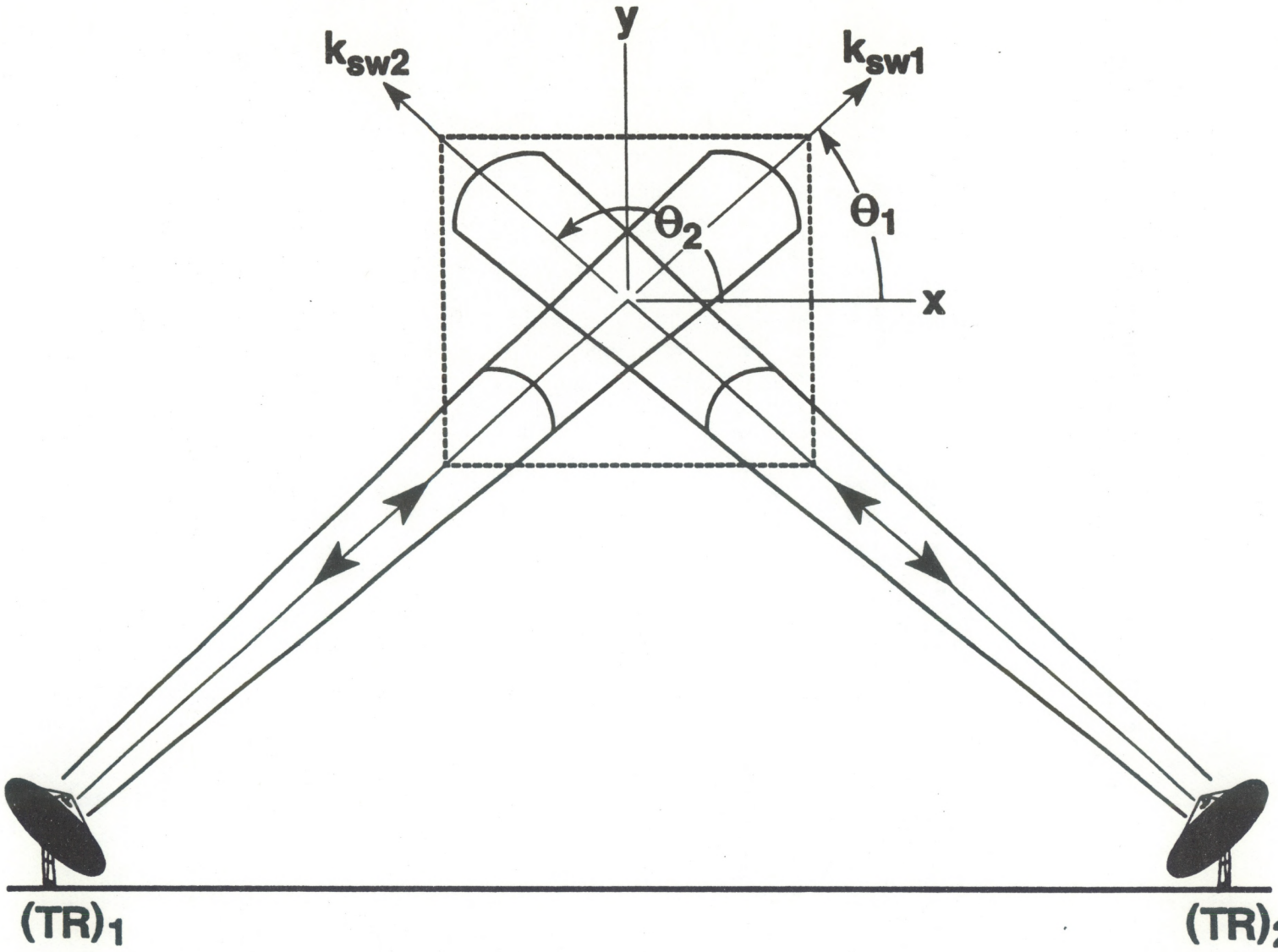

Figure 5. Two-station, dual-frequency radar sensing of an ocean surface current vector field. The dotted line indicates the spatial resolution.

$$\delta v_x = \frac{\left[(\delta v_1)^2 \sin^2(\theta_2) + (\delta v_2)^2 \sin^2(\theta_1)\right]^{1/2}}{\left|\sin(\theta_2 - \theta_1)\right|} \tag{32}$$

$$\delta v_y = \frac{\left[(\delta v_1)^2 \cos^2(\theta_2) + (\delta v_2)^2 \cos^2(\theta_1)\right]^{1/2}}{\left|\sin(\theta_2 - \theta_1)\right|} \tag{33}$$

Equations (32) and (33) can now be used in combination with Eq. (23) to plot a map of the surface current vector field resolution achievable with a two-station Δk-radar system. These formulae were evaluated numerically for the ocean surface conditions selected in Table 1 and for a beamwidth of 0.8°. A contour plot of the surface current resolution for these conditions is presented in Fig. 6. The locations of the dual-frequency transmitters and receivers are illustrated on the plots by the symbols T and R, respectively, and the plotted current resolution is the larger of δv_x and δv_y.

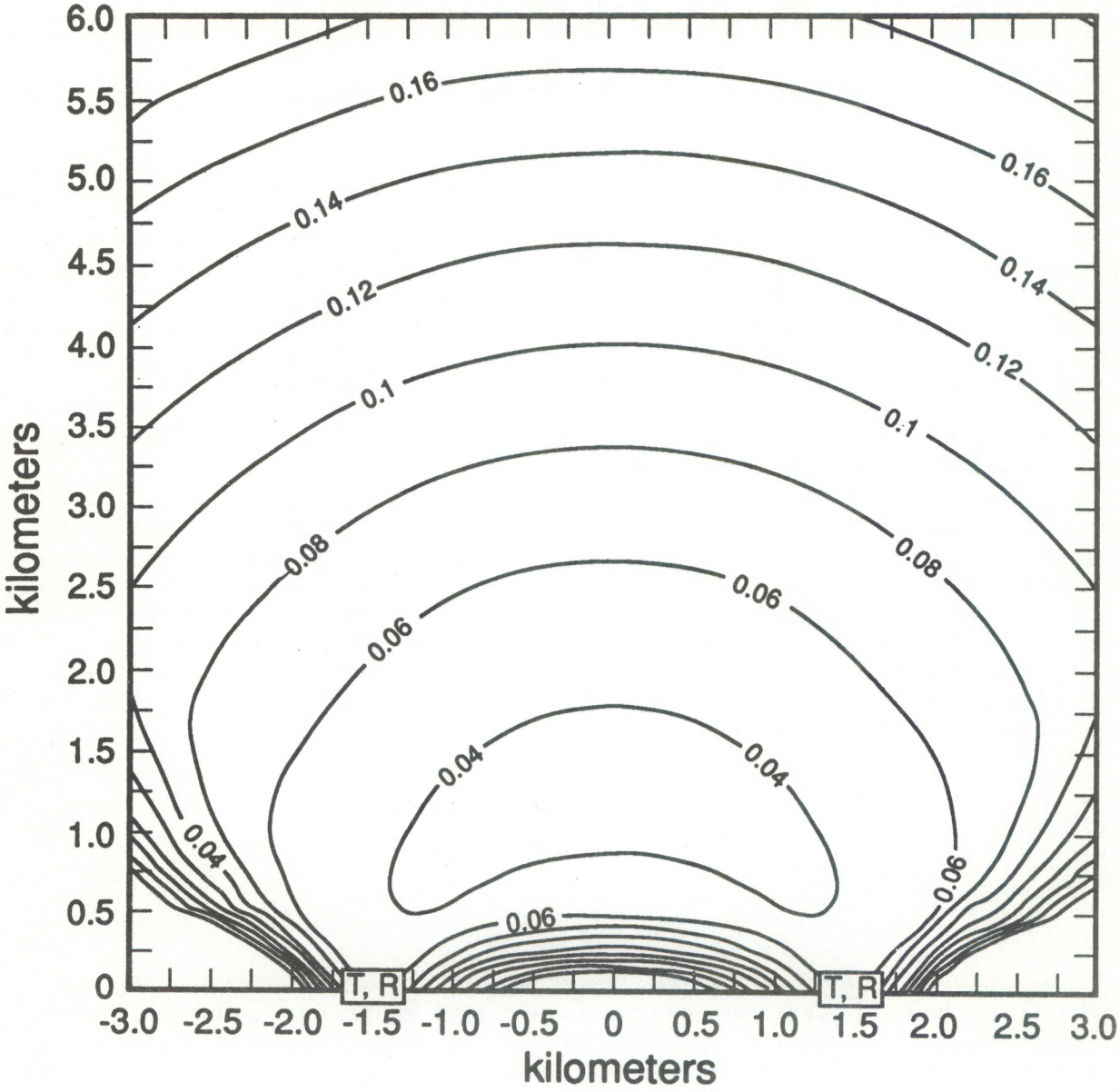

Figure 6. Contour map of achievable surface current resolution in m/sec under conditions specified in Table 1 for a two-station monostatic dual-frequency radar. T and R indicate locations of dual-frequency transmitters and receivers, respectively.

4. POSSIBLE NEW APPROACHES

4.1 Bistatic Dual-Frequency Radar

The use of bistatic Doppler radar configurations for mapping velocity fields is usually impractical for atmospheric applications because of the precision aiming and registration requirements necessitated by the high gains of the receiving antennas. High antenna gains are necessary for atmospheric applications because of the relatively low radar cross sections and large ranges that are involved. On the other hand, in land-based radar sensing of the ocean surface, the ranges are much shorter and the radar cross sections are much larger. The consequent relaxation of the requirement for high receiver antenna gains may make the use of a bistatic radar mode practical for obtaining additional ocean surface current components.

The signal-to-noise ratio discussed in the above sections cannot be used to determine the required antenna gains because it is determined by the spectral scattering properties of the ocean surface, and is independent of the transmitted and received power levels. The noise source that can be used to determine the required antenna gains is thermal noise in the receiver. The signal-noise-ration determined by this noise source is given by the radar range equation:

$$S/N|_{rcvr} = \frac{P G_T G_R \lambda_i^2 \Delta r \phi \sigma}{[(4\pi)^3 NP\, LF\, r^3]} \qquad (34)$$

Here P is the average transmitter power; λ_i is the radar wavelength; G_T and G_R are the transmitter and receiver antenna gains, respectively; Δr is the radial extent of the resolved pixel; r is its range; ϕ is the transmitting antenna beam width; (NP) is the thermal noise power of the receiver; LF is the total system loss factor; and σ is the radar cross section per unit area of the ocean surface.

The radar cross section per unit area for the ocean surface is approximately -25 dB for centimeter waves. This cross section falls sharply for grazing angles lower than about 0.5°. This will limit the maximum range over which a land-based Δk radar can achieve a detectable return. Even for a high cliff-based radar, say, 300 m above the ocean surface, this corresponds to a maximum range of only about 30 km.

If we select this maximum possible range together with the set of typical radar system parameters given in Table 2, and the set of nominal ocean surface parameters given in Table 1, we may estimate how small the receiver antenna gain could be while still maintaining the receiver signal-to-noise ratio above the spectral clutter induced signal-to-noise ratio. With these substitutions in Eqs. (8), (23), (25), and (34), we find that the receiver antenna gain could be as low as minus 20 dB before the receiver signal-to-noise ratio dropped below the clutter induced signal-to-noise ratio.

Table 2: Radar system parameters used for computation of minimuim receiver antenna gain.

λ_i	.03 m
P	30 W
ϕ	0.8°
G_T	40 dB
NP	1×10^{-21} W
LF	1
Δr	0.1 km
n	1

Thus, the detectability of the Δk-radar signals will be limited by clutter noise even with the use of omnidirectional receiving antennas. This fact justifies the concept of a bi-static dual-frequency radar for measuring ocean surface currents. Elsewhere[7] we have computed the achievable resolution of an ocean surface current field using a dual-frequency radar system in a combined monostatic and bistatic configuration. Fig. 7 displays a contour map of surface current resolution from that work for the bistatic case for the same conditions assumed for the mono-static contour map of Fig. 6. To facilitate comparison with the monostatic case, a three station configuration is assumed for the bistatic case to exhibit the same symmetry as the two-station monostatic case. As shown, the bistatic current resolution is about twice that of the corresponding monostatic case.

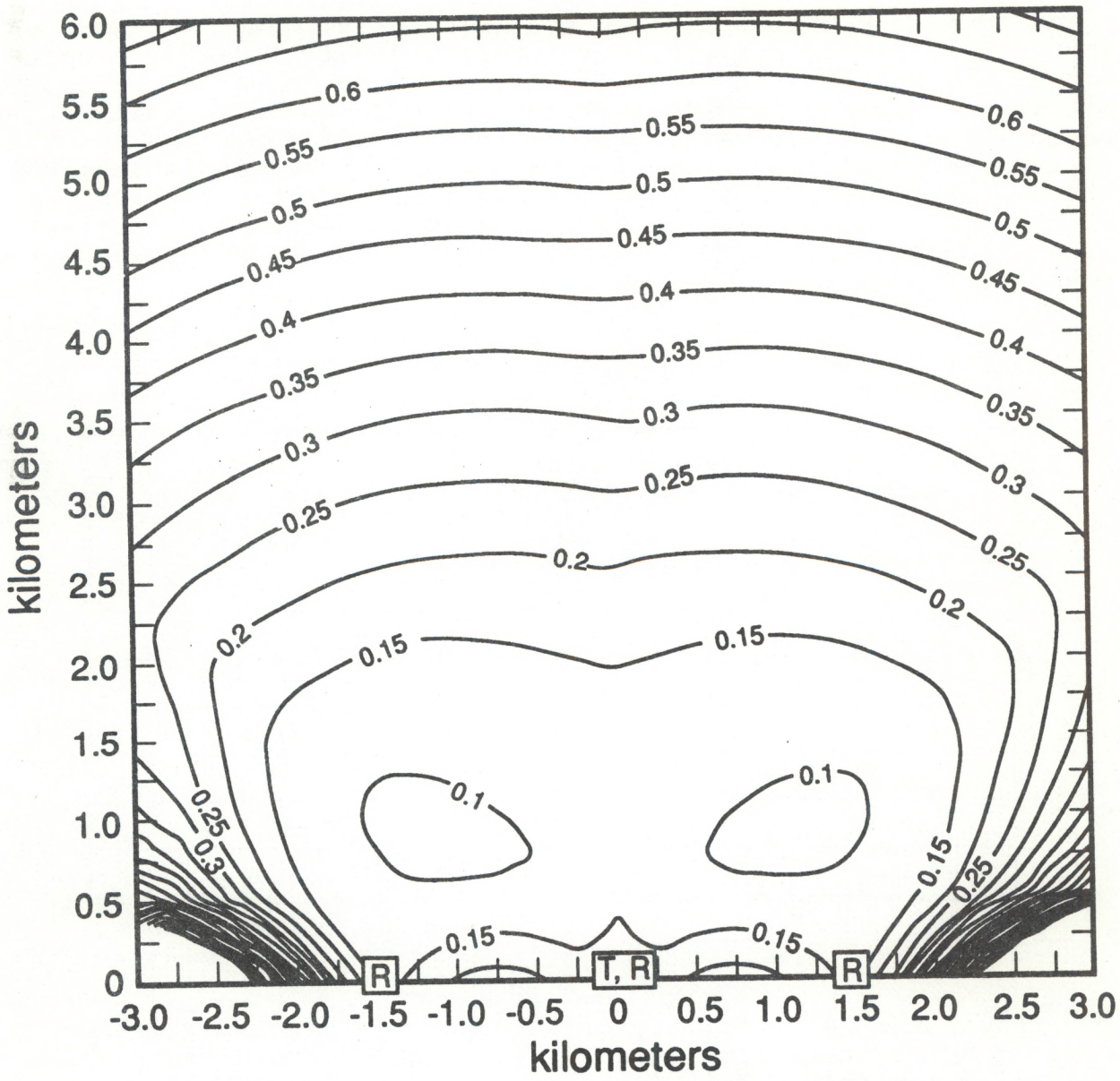

Figure 7. Contour map of achievable surface current resolution in m/sec under conditions specified in Table 1 for a three-station combined monostatic and bistatic dual-frequency radar. T and R indicate locations of the dual-frequency radar. T and R indicate locations of the dual-frequency transmitters and receivers, respectively.

The improved resolution capability of the monostatic system is due to three factors. One factor is the somewhat shorter ranges involved in the monostatic case. Another factor the greater angular separation between the detected current components for the monostatic system. The third factor is the larger average coherence length of the detected swell in the monostatic case[7].

It is important to recognize that the two compared configurations achieve different spatial resolutions. In the bistatic configuration the illuminated area which defines the spatially resolved pixel is simply the antenna pattern of the single transmitted beam (or range gate) onto the surface. On the other hand, the monostatic configuration requires two transmitted beams and the resolved pixel is determined by the intersection of the two projected beam patterns as illustrated in Fig. 8. For beam patterns which are long in the radial direction compared to the azimuthal direction, which is necessary to achieve the best current resolution, the bistatic configuration will, as illustrated, achieve a finer spatial resolution.

The primary advantage of the bistatic configuration is cost reduction by eliminating the need for an additional transmitter. The comparisons presented above can be used to help asses whether, for a particular application, the better current resolution for the monostatic configuration justifies its additional cost.

4.2 Dual-Frequency Sodar

Frisch and Clifford[8] have proposed a dual-frequency sodar concept completely analogous to the dual-frequency radar technique reviewed above except that acoustic radiation is used instead of electromagnetic radiation. Under the conditions where the spectral properties of the ocean surface dominate the signal to noise ratio, the entire performance analysis reviewed above for dual-frequency radar sensing of ocean surface currents applies equally to dual-frequency sodar sensing of ocean surface currents. This is because the speed of light does not enter into the analysis other than in the dispersion relationship for the radiation. It is possible that the modulation transfer function for acoustic radiation, which enters the expression for the clutter induced signal to noise ratio, might differ slightly from that for electromagnetic radiation due to the polarization difference.

The principal difference between Δk-sodar and Δk-radar is the system signal-to-noise ratio given by the radar-range equation, Eq. (34). This difference is due primarily to the increased noise power, NP, for sodar. The propagation loss which contributes to the loss factor, LF, will also be larger for

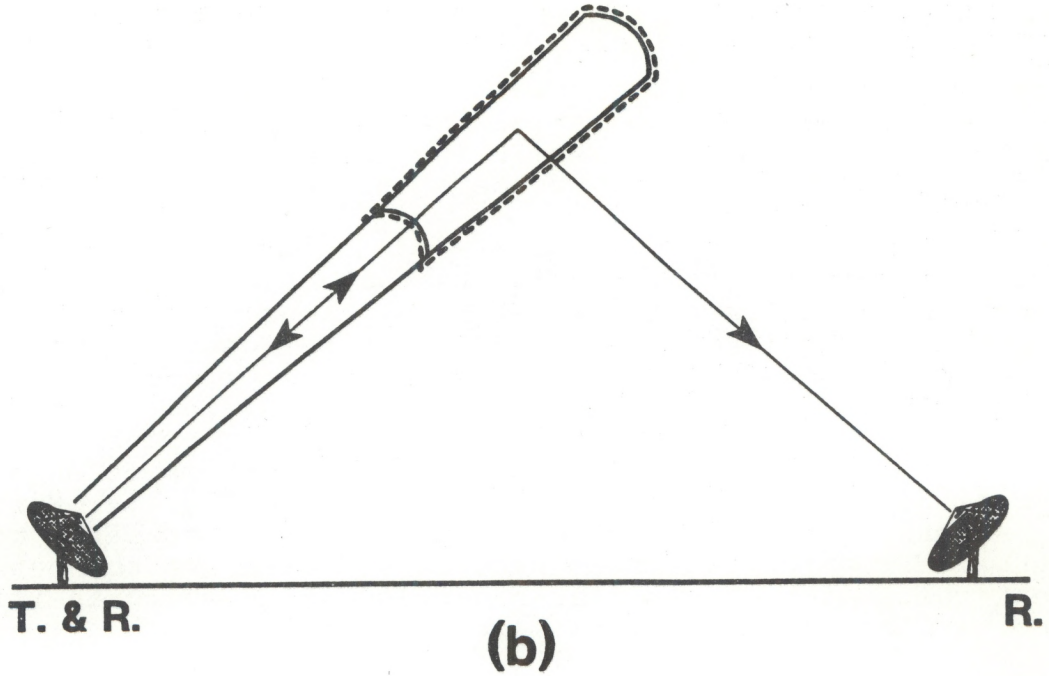

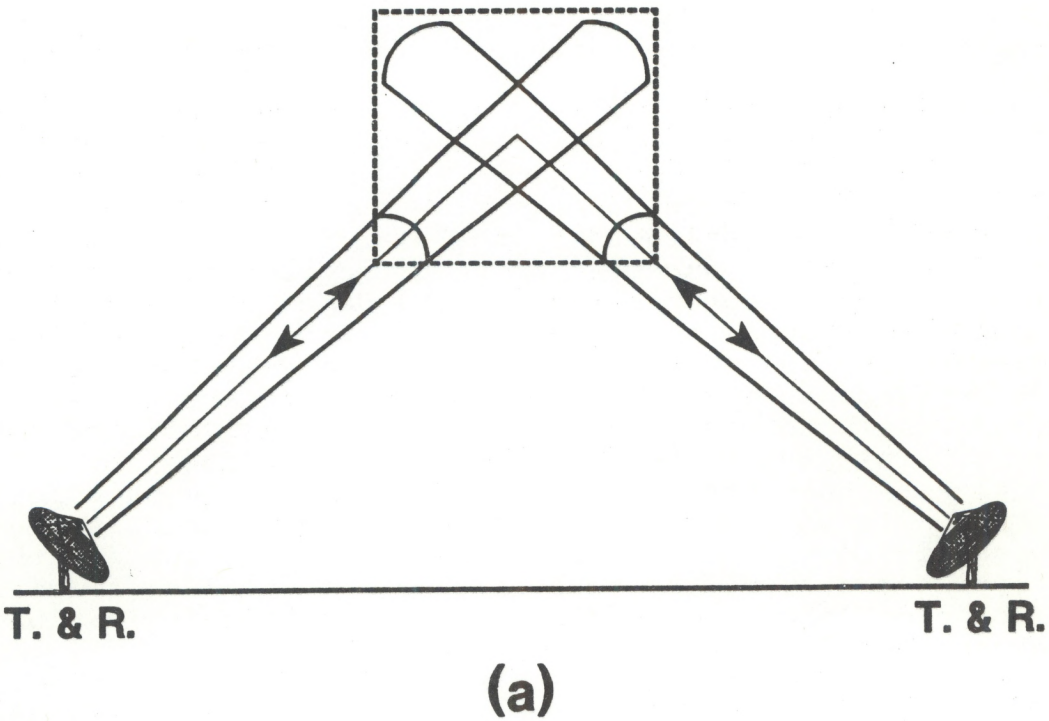

Figure 8. Spatially resolved pixel for: (a) a monostatic, dual-frequency radar using two transmitting stations; and (b) a combined monostatic and bistatic configuration using only one transmitting station.

sodar. The increased loss will be caused by absorption as well as by beam steering and scattering caused by temperature gradients near the ocean surface (for above surface applications). In our estimate for the sodar system signal to noise ratio, we will neglect any propagation loss and continue to assume LF = 1, thus obtaining a best-case estimate for the system signal-to-noise ratio.

The dominant source of system noise for Δk-sodar is ambient background noise entering the receiver antenna (rather than internal thermal noise which is the case for radar.) This external noise power can be written

$$NP = p_{amb} (\Delta\Omega/4\pi) A B \tag{35}$$

where A is the receiver antenna area, $\Delta\Omega$ is the received solid angle, B is the receiver bandwidth, and p_{amb} is the ambient noise power density per unit frequency of bandwidth received by an omnidirectional antenna. For circular aperture antennas,

$$\Delta\Omega = (\pi/4) (\lambda^2/A) \tag{36}$$

So Eq. (35) can be written

$$NP = \frac{p_{amb} B \lambda^2}{16} \tag{37}$$

For frequencies near 1 kHz, a typical value for p_{amb} in air[9] is $p_{amb} \sim 1 \times 10^{-15}$ W/(cm^2·Hz), while for shallow ocean water[10], $p_{amb} \sim 10^{-13}$ W/(cm^2·Hz). For a one hertz bandwidth appropriate to Δk-sodar signal processing, the corresponding 1 kHz noise powers are:

$$NP_{air} \sim 10^{-13} W \tag{38}$$

$$NP_{water} \sim 10^{-10} W \tag{39}$$

These noise powers are 80 - 110 dB larger than the noise power of a typical x-band radar receiver. Assuming that the remaining parameters that enter the radar range equation are the same as assumed for the radar case (Table 2), and assuming a 40 dB gain

equal to that assumed for the radar case (-25 dB), Eq. (34) gives a maximum range for maintaining the Δk-sodar system signal to noise ratio above 10 dB as

$$R_{air} < 100km \tag{40}$$

$$R_{water} < 20km \tag{41}$$

These best case maximum ranges exceed the attenuation length for the sodar signals so ambient noise does not appear to be a limiting factor for the Δk-sodar concept. Indeed, for ranges of a few kilometers ambient noise will evidently remain acceptable for receiver antenna gain near unity which would allow for the possibility of the a bistatic Δk-sodar configuration.

5.0 REFERENCES

1. W. J. Plant, "Studies of backscattered sea return with a CW, dual-frequency, X-band radar," *IEEE Trans. Antennas Propag.*, **AP-25**, 28-36 (1977).

2. W.J. Plant and D.L. Schuler, "Remote sensing of the sea surface using one and two frequency microwave techniques," *Radio Sci.* **15**, 605 - 615 (1980).

3. W. Alpers and K. Hasselmann, "The two-frequency microwave technique for measuring ocean-wave spectra from an airplane or satellite," *Bound.-Layer Meteor.*, **13**, 215-230 (1978).

4. R.E. McIntosh, C.T. Swift, R.S. Rughavan, and A.W. Baldwin, "Measurement of ocean surface currents from space with multifrequency radars—a system analysis," *IEEE Trans. Geosci. Remote Sens.*, **GE-23**, 2-12 (1984).

5. D.L. Schuler, W.J. Plant, A.B. Reeves, and W.P. Eng, "Removal of clutter background limitations in dual-frequency scattering from the ocean," *Int. J. Remote Sens.*, **6**, 1091-1112 (1985).

6. A.S. Frisch and J. Leise, "A note on using continuity to extend HF radar surface-current measurements," *J. Geophys. Res.*, **86**, 11089-11090 (1981).

7. A.J. Palmer, "A bi-static dual-frequency radar concept for measuring ocean surface currents," (submitted to *IEEE Trans. Geosci. Remote Sens.*, 1990).

8. A.S. Frisch and S.F. Clifford, "An acoustic remote sensor of ocean current and wave spectra," NOAA Wave Propagation Laboratory Patent Disclosure, (1989).

9. A.J. Bedard (private communication).

10. R.J. Urich, *Principles of Underwater Sound*, McGraw-Hill, New York (1983).

☆U.S. GOVERNMENT PRINTING OFFICE: 1990 - 573-002/21015